The Planetary Science Journal, 3:133 (16pp), 2022 June https://doi.org/10.3847/PSJ/ac6ce2

Free Core Nutation and Its Relation to the Spin-over Mode

Jérémy Rekier
Royal Observatory of Belgium Avenue circulaire, 3 B-1180 Brussels, Belgium; jeremy.rekier@observatory.be
Received 2022 January 25; revised 2022 May 2; accepted 2022 May 3; published 2022 June 6

Abstract

The time-varying response of Earth's and other planets' rotation to external gravitational torques depends strongly on their internal structure. In particular, the existence of the mode known as the free core nutation in the fluid core is known to amplify the forced nutations in the near-diurnal retrograde frequency band (as measured in the planetary frame of reference). Due to their proximity in shape and frequency, this mode is sometimes equated with the so-called spin-over mode, which denotes the free oscillation of a steadily rotating ellipsoidal fluid core. Through a careful study of the freely rotating two-layer planetary model with a rigid mantle and an inviscid fluid core, we show that the spin-over mode frequency corresponds to that where the sum of the external and internal torques on the mantle is balanced, causing it to rotate steadily. The presence of dissipation at the core−mantle boundary causes the free core nutation to become damped and slightly offsets its resonance frequency. We show that this offset, which is ≈ -1 day for Earth, can be interpreted as the result of the proximity of the free core nutation frequency to that of the spin-over mode, which now corresponds to a minimum in the magnitude of the transfer function for nutations. We also show how this proximity leads to a slightly lower quality factor for the resonance than that computed from the usual formula. We conclude by discussing possible implications of this mechanism for Mars, the Moon, and the long-term evolution of Earth.

Unified Astronomy Thesaurus concepts: Earth (planet) (439); Solar system (1528); Mars (1007); The Moon (1692); Geodesics (645); Lunar geodesy (955)

1. Introduction

The orientation of Earth in space varies in time under the influence of gravitational attraction, primarily by the Sun and Moon, resulting in the motion of its rotation axis known as *precession-nutation*. In the frequency domain, nutation is composed of a wide array of terms—collectively referred to by the plural *nutations*—with small amplitude and high frequency compared to the larger, slower precession. The nutation amplitudes depend strongly on the planet's internal structure. In particular, Earth's liquid core is known to amplify nutations in the retrograde near-diurnal frequency band, as measured in the terrestrial reference frame (see later). This amplification is due to the existence of the free rotational mode known as the *free core nutation* (FCN) inside the fluid core and coupled to the rotation of Earth's solid mantle via the pressure torque it exerts on the oblate core–mantle boundary (CMB; Dehant & Mathews 2015b). Such a liquid core is not unique to Earth but most likely exists in all known terrestrial planets, as well as in the Moon, which must therefore also possess an FCN.

Planets liquid cores are an ideal subject for the study of rotating fluids given the importance of the *Coriolis force* in these objects. One example is the way this force combines with the convective motion in Earth's core to generate its self-sustaining magnetic field in a complex process known as the *geodynamo*. Already at the linear level, the Coriolis force can act as the restoring force generating oscillations known as *inertial waves* in planetary fluid cores (Greenspan 1968). From a mathematical perspective, it was recently shown that these waves form a complete flow basis in inviscid fluids enclosed within an ellipsoidal CMB, thereby motivating the term *inertial modes*, which is also employed for viscous fluids, by extension (Ivers et al. 2015; Backus & Rieutord 2017; Ivers 2017).

From laboratory experiments, we know that inertial modes can be excited in many different ways (Le Bars et al. 2015). Among existing mechanisms, precession of the container's orientation is particularly interesting given its similarities with Earth's precession-nutation. Since the work of Poincaré (1910), such forcing is known to excite a simple inertial mode characterized by its near-diurnal frequency and its uniform vorticity parallel to the planet's equatorial plane, when observed from the terrestrial reference frame, later baptized the *spin-over mode* (SOM). Because this mode shares its two defining characteristics with the FCN, the two have sometimes been identified as one and the same thing. To make matters worse, the similarity in name with yet another mode, known as the *tilt-over mode* (TOM), has sometimes led to the three terms being used interchangeably (see, e.g., Toomre 1974; Noir et al. 2003; Cébron et al. 2010, or recently Nobili et al. 2021), causing some confusion between the fluid dynamics and geodesist communities.

Some attempts to clarify this use of vocabulary have been made recently, starting with the work of Triana et al. (2019), who studied the dynamics of viscous inertial modes coupled to planetary rotation and showed how the FCN coincides with the SOM, only in the limit where the planet rotates steadily around its axis. Rekier et al. (2020) gave a simplified description of the same problem for the inviscid fluid and formally showed how the FCN is the direct generalization of the SOM for a freely rotating planet, as well as the only inertial mode affected by the nonsteady rotation in the inviscid case. That work can be seen, in large part, as an update to Hough (1895), who had already presented many of the same arguments using a somewhat dated formalism.

In the present paper, we elaborate on these previous works and present a detailed analysis of the rotating two-layer

planetary model subjected to external gravitational forcing, carried out in Section 2. We find that while the SOM does indeed disappear from the spectrum in favor of the FCN for a freely rotating planet, its frequency retains some significance and corresponds to that where the amplitudes of the forced nutations become zero when there is no dissipation at the CMB. We show how this result follows naturally from the usual understanding of the SOM. We also give a detailed description of the TOM and the way it differs from the SOM and FCN, in an attempt to remove the confusion between these names.

As the frequencies of the SOM and FCN are typically very close to each other, the amplitudes of the forced nutations vary from zero to infinity in a very narrow frequency band in the idealized nondissipative model. In Section 3 we reintroduce the effects of the mantle's elasticity, as well as the additional dissipative couplings at the CMB. This coupling causes the FCN to become a damped mode and to increase its frequency (in absolute value), as is well known. The damping itself further contributes to slightly offseting the resonance frequency of the nutations compared to the FCN. By considering the representation of the system in terms of its complex transfer function, we show in Section 4 that this offset can be interpreted as a consequence of the proximity between the FCN and the SOM frequencies. We evaluate this offset to be of the order of ≈ -1 day in period for Earth, and likely much smaller for Mars. We conclude with possible implications for the Moon and Earth's long-term evolution.

2. Two-layer Planetary Model

2.1. Equations of Motion

The *Liouville equations* governing the rotation of a two-layer planet are written as

$$\frac{d\boldsymbol{H}_{\rm m}}{dt} + \boldsymbol{\Omega} \times \boldsymbol{H}_{\rm m} = \boldsymbol{\Gamma}_{\rm m} + \boldsymbol{\Gamma}_{\rm f\to m}, \tag{1}$$

$$\frac{d\boldsymbol{H}_{\rm f}}{dt} + \boldsymbol{\Omega} \times \boldsymbol{H}_{\rm f} = \boldsymbol{\Gamma}_{\rm f} + \boldsymbol{\Gamma}_{\rm m\to f}, \tag{2}$$

$$\frac{d\boldsymbol{H}}{dt} + \boldsymbol{\Omega} \times \boldsymbol{H} = \boldsymbol{\Gamma}, \tag{3}$$

where $\boldsymbol{H}_{\rm m}$ and $\boldsymbol{H}_{\rm f}$ denote the angular momentum of the mantle and core, respectively, which must add up to the total angular momentum of the whole planet: $\boldsymbol{H} = \boldsymbol{H}_{\rm m} + \boldsymbol{H}_{\rm f}$. Likewise, $\boldsymbol{\Gamma}_{\rm m}$ and $\boldsymbol{\Gamma}_{\rm f}$ respectively denote the torques exerted on the mantle and core by external sources and must satisfy $\boldsymbol{\Gamma} = \boldsymbol{\Gamma}_{\rm m} + \boldsymbol{\Gamma}_{\rm f}$, where $\boldsymbol{\Gamma}$ denotes the total torque from external sources. Conservation of angular momentum further imposes that Equations (1) and (2) must add up to Equation (3), so that

$$\boldsymbol{\Gamma}_{\rm m\to f} + \boldsymbol{\Gamma}_{\rm f\to m} = \boldsymbol{0}, \tag{4}$$

i.e., the torque exerted by the mantle on the fluid core must balance that exerted by the core on the mantle. In Equations (1) to (3), $\boldsymbol{\Omega}$ denotes the angular velocity of the reference frame, with respect to the inertial frame. It is often convenient to work in the so-called *mantle frame*, where the mantle appears at rest, and to use a Cartesian coordinate basis, $\{\hat{\boldsymbol{x}}, \hat{\boldsymbol{y}}, \hat{\boldsymbol{z}}\}$, aligned with the principal axes of inertia of both the core and mantle—which are assumed identical. For the axisymmetric planet, the tensor of inertia of the whole planet and its fluid core, respectively, read

$$\underline{\boldsymbol{I}} = A\,(\hat{\boldsymbol{x}}\hat{\boldsymbol{x}} + \hat{\boldsymbol{y}}\hat{\boldsymbol{y}} + (1+e)\hat{\boldsymbol{z}}\hat{\boldsymbol{z}}), \tag{5}$$

$$\underline{\boldsymbol{I}}_{\rm f} = A_{\rm f}(\hat{\boldsymbol{x}}\hat{\boldsymbol{x}} + \hat{\boldsymbol{y}}\hat{\boldsymbol{y}} + (1+e_{\rm f})\hat{\boldsymbol{z}}\hat{\boldsymbol{z}}), \tag{6}$$

where expressions of the form $\hat{\boldsymbol{x}}\hat{\boldsymbol{x}}$ denote the direct (dyadic) product of the unit vector, $\hat{\boldsymbol{x}}$, with itself. The real quantities $e > 0$ and $e_{\rm f} > 0$ are the *dynamical flattenings* of the whole planet and its fluid core, respectively. The tensors of inertia satisfy $\underline{\boldsymbol{I}} = \underline{\boldsymbol{I}}_{\rm f} + \underline{\boldsymbol{I}}_{\rm m}$, where $\underline{\boldsymbol{I}}_{\rm m}$ is the tensor of inertia of the mantle. The latter being solid, its angular momentum can be expressed in terms of its angular velocity, $\boldsymbol{\Omega}$, via

$$\boldsymbol{H}_{\rm m} = \underline{\boldsymbol{I}}_{\rm m} \cdot \boldsymbol{\Omega}. \tag{7}$$

In the study of planetary rotation, one focuses on small oscillations about a steady state chosen along the z-axis:

$$\boldsymbol{\Omega} = \Omega_0(\hat{\boldsymbol{z}} + \boldsymbol{m}), \tag{8}$$

where Ω_0 is the diurnal *spin rate*. The vector, $\boldsymbol{m}$, is called the mantle's *wobble* and satisfies $|\boldsymbol{m}| \ll 1$. For Earth, its components are typically of the order of 10^{-8} to 10^{-6}. It is sometimes useful to know the mantle's velocity with respect to some intermediate frame rotating steadily at diurnal frequency around the vertical axis, $\hat{\boldsymbol{Z}}$, chosen along the mean polar axis of the planet in the inertial frame, hereafter denoted as the *steadily rotating frame* (SRF). The dynamical relations between this frame, the mantle frame, and the inertial frame are given in Appendix A. The angular velocity of the mantle in the SRF reads

$$\begin{aligned}\boldsymbol{\Omega}_{\rm srf} &= \boldsymbol{\Omega} - \Omega_0\hat{\boldsymbol{Z}} \\ &= \Omega_0(\hat{\boldsymbol{z}} - \hat{\boldsymbol{Z}}) + \Omega_0\boldsymbol{m}.\end{aligned} \tag{9}$$

In principle, the angular momentum of the fluid core must be computed from the flow velocity. However, it can be shown that—in the special case of an ellipsoidal CMB—this velocity can be decomposed as

$$\boldsymbol{v} = \boldsymbol{\omega}_{\rm f} \times \boldsymbol{r} + \boldsymbol{\nabla}\psi, \tag{10}$$

where $\boldsymbol{v}$ denotes the flow velocity with respect to the mantle frame and $\boldsymbol{\omega}_{\rm f}$ is the *mean flow rotation*, satisfying $\boldsymbol{\nabla} \times \boldsymbol{v} = 2\boldsymbol{\omega}_{\rm f}$. By analogy with Equations (8), and (9), we write

$$\boldsymbol{\omega}_{\rm f} = \Omega_0\boldsymbol{m}_{\rm f}, \tag{11}$$

$$\begin{aligned}\boldsymbol{\omega}_{\rm f|srf} &= \boldsymbol{\Omega}_{\rm srf} + \boldsymbol{\omega}_{\rm f} \\ &= \Omega_0(\hat{\boldsymbol{z}} - \hat{\boldsymbol{Z}}) + \Omega_0(\boldsymbol{m} + \boldsymbol{m}_{\rm f}),\end{aligned} \tag{12}$$

where $\boldsymbol{\omega}_{\rm f|srf}$ denotes the fluid's angular velocity with respect to the SRF and $|\boldsymbol{m}_{\rm f}| \ll 1$. Equation (10) was first given—in a different form—by Poincaré (1910), who also showed that the contribution of the second term of this equation to the core angular momentum was of the second order in the core flattening and could therefore be neglected in front of the other term in planetary applications. The angular momentum of the core and the whole planet may therefore respectively be written as

$$\boldsymbol{H}_{\rm f} \approx \underline{\boldsymbol{I}}_{\rm f} \cdot (\boldsymbol{\Omega} + \boldsymbol{\omega}_{\rm f}), \tag{13}$$

$$\boldsymbol{H} \approx \underline{\boldsymbol{I}} \cdot \boldsymbol{\Omega} + \underline{\boldsymbol{I}}_{\rm f} \cdot \boldsymbol{\omega}_{\rm f}, \tag{14}$$

which are valid to order $\mathcal{O}(|{\rm m}|e_{\rm f})$.

Of Equations (1)–(3), only two are independent. The traditional choice is to solve Equation (3) together with a modified version of Equation (2) first proposed by Sasao et al. (1980), who showed that it could be advantageously replaced by

$$\frac{d\boldsymbol{H}_{\rm f}}{dt} - \boldsymbol{\omega}_{\rm f} \times \boldsymbol{H}_{\rm f} \approx \boldsymbol{0}, \tag{15}$$

which avoids having to evaluate $\boldsymbol{\Gamma}_{\rm m\to f}$ explicitly. Equation (15) is valid to the same order of approximation as Equations (13) and (14), provided that $\boldsymbol{\Gamma}_{\rm m\to f}$ is limited to the sum of the pressure and gravitational torques exerted by the mantle on the fluid. We will relax this assumption in Section 3.3 below.

Finally, the total torque acting on the planet is the sum of the individual contributions from external gravitational forces and reads

$$\boldsymbol{\Gamma} = -\int_{\mathcal{V}} \rho \boldsymbol{r} \times \boldsymbol{\nabla}\phi \, dV, \tag{16}$$

where the integral runs over the volume $\mathcal{V}$ of the whole planet, ρ is the mass density, and ϕ is the total gravitational potential. For an axisymmetric planet, and to first order in e, the two equatorial components of Equation (16) in the body frame can be combined as (Mathews et al. 1991)

$$\tilde{\Gamma} = iAe\tilde{\phi}, \tag{17}$$

where we have defined $\tilde{\Gamma} \equiv \Gamma^x + i\Gamma^y$, and where $\tilde{\phi}$ is proportional to the coefficient of the degree-2, tesseral spherical harmonics expansion of ϕ.

From the above, the equatorial components of the wobble, m^x and m^y, can be shown to decouple from the axial component m^z, to first order in $\boldsymbol{m}$, and similarly for the components of $\boldsymbol{m}_{\rm f}$. After solving for these vector components in the mantle frame, we can use the solution to compute the kinetic energy of the mantle and core. In practice, it will often prove useful to do so in the SRF, where they are defined as

$$E^{\rm m}_{\rm kin} = \frac{1}{2}\boldsymbol{\Omega}^{\top}_{\rm srf} \cdot \underline{\boldsymbol{I}}_{\rm m} \cdot \boldsymbol{\Omega}_{\rm srf}, \tag{18}$$

$$E^{\rm f}_{\rm kin} = \frac{1}{2}\boldsymbol{\omega}^{\top}_{\rm f|srf} \cdot \underline{\boldsymbol{I}}_{\rm f} \cdot \boldsymbol{\omega}_{\rm f|srf}. \tag{19}$$

2.2. Prograde and Retrograde Motions (Sign Conventions)

The wobbly motion of an axisymmetric planetary model can be written as a circular rotation of the vector, $\boldsymbol{m}$, within the equatorial plane at constant angular frequency, ω:[1]

$$\begin{pmatrix} m^x \\ m^y \end{pmatrix} = \underbrace{\begin{pmatrix} \cos\omega t & -\sin\omega t \\ \sin\omega t & \cos\omega t \end{pmatrix}}_{R(t)} \begin{pmatrix} m^x_0 \\ m^y_0 \end{pmatrix}, \tag{20}$$

where m^x_0 and m^x_0 are the values of m^x and m^y at $t = 0$. The *canonical basis* offers a useful way to diagonalize the relation given by Equation (20). It is defined in terms of the Cartesian basis as

$$\begin{pmatrix} \hat{\epsilon}_- \\ \hat{\epsilon}_+ \end{pmatrix} = \underbrace{\frac{1}{\sqrt{2}}\begin{pmatrix} 1 & -i \\ -1 & -i \end{pmatrix}}_{P} \begin{pmatrix} \hat{\boldsymbol{x}} \\ \hat{\boldsymbol{y}} \end{pmatrix}. \tag{21}$$

It is then straightforward to show that the equatorial components of $\boldsymbol{m}$ along $\hat{\epsilon}_-$ and $\hat{\epsilon}_+$ satisfy

$$\begin{pmatrix} m^- \\ m^+ \end{pmatrix} = P^* R(t) P^{\top} \begin{pmatrix} m^-_0 \\ m^+_0 \end{pmatrix}, \tag{22}$$

where * denotes the complex conjugate. Upon defining $\tilde{m} \equiv (m^x + im^y) = \sqrt{2}\ m^-$, we finally obtain

$$\begin{pmatrix} \tilde{m} \\ \tilde{m}^* \end{pmatrix} = \begin{pmatrix} e^{i\omega t} & 0 \\ 0 & e^{-i\omega t} \end{pmatrix} \begin{pmatrix} \tilde{m}_0 \\ \tilde{m}^*_0 \end{pmatrix}. \tag{23}$$

From Equation (23), we see that $\tilde{m}$ and $\tilde{m}^*$ rotate in opposite directions in the complex plane. For $\omega > 0$, $\tilde{m}$ describes a *prograde* motion and $\tilde{m}^*$ describes a *retrograde* motion with the same angular velocity. The opposite is true when $\omega < 0$. We also see that the dynamics of $\tilde{m}$ and $\tilde{m}^*$ decouple for a circular motion. This allows us to focus exclusively on $\tilde{m}$ in what follows. However, based on the above, it should be kept in mind that, in order for a general solution of Equation (20) to be real-valued, to each particular solution, $\tilde{m}_0(\omega)e^{i\omega t}$, there must correspond another particular solution with opposite frequency: $\tilde{m}^*_0(-\omega)e^{-i\omega t}$. Both solutions describe the same physical prograde or retrograde motion.

In what follows, we drop the subscript notation for readability and use the same symbol, $\tilde{m}$, to denote both the wobble component and its *Fourier mode*, $\tilde{m}_0(\omega)$.

2.3. Solution for a Rigid Mantle

In the rest of this work, we use units in which the (prograde) diurnal frequency has the numerical value $\Omega_0 = 1$, and all frequencies are given in cycles per day (cpd), unless otherwise mentioned. Based on the above considerations, Equations (3) and (15) can be summarized in the following matrix form:

$$\begin{pmatrix} \omega - e & (1+\omega)\dfrac{A_{\rm f}}{A} \\ \omega & \omega + (1 + e_{\rm f}) \end{pmatrix} \begin{pmatrix} \tilde{m} \\ \tilde{m}_{\rm f} \end{pmatrix} = \begin{pmatrix} e\tilde{\phi} \\ 0 \end{pmatrix}, \tag{24}$$

where $\tilde{m}_{\rm f} \equiv (m^x_{\rm f} + im^y_{\rm f})$ is analogous to $\tilde{m}$ for the fluid core.

Equation (24) reflects an important property already identified by Poincaré (1910), who noticed that when $\omega = -1$ the dynamics of $\tilde{m}$ becomes independent of $\tilde{m}_{\rm f}$, so that the wobble of the two-layer model is governed by the same equation as for a single-layer *rigid* planet:

$$(\omega - e)\tilde{m} = e\tilde{\phi}. \tag{25}$$

Poincaré named this phenomenon *gyrostatic rigidity* and showed how it is related to the existence of a particular type of rotational mode, which was later called the TOM (see Section 2.4 below). The solution to Equation (25) is written as

$$\tilde{m}_R(\omega) = \frac{e\tilde{\phi}}{(\omega - e)}, \tag{26}$$

where the subscript is a reminder that Equation (26) is only valid for a single-layer rigid planet for $\omega \neq -1$. This solution

[1] Note that this is *not* true for a nonaxisymmetric planet (see, e.g., Dehant & Mathews 2015b).

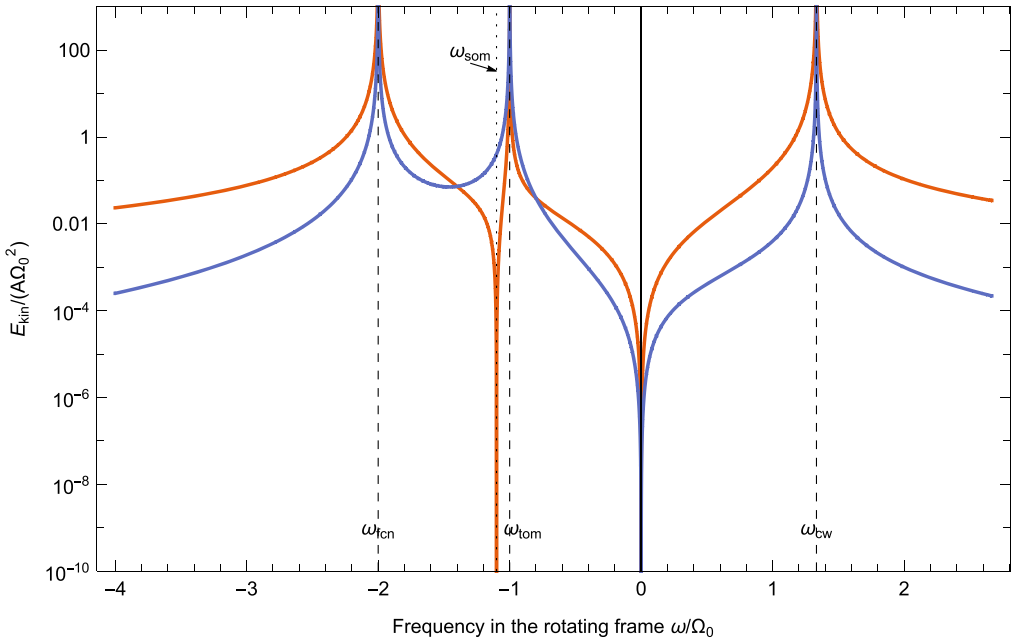

Figure 1. Normalized kinetic energy of the mantle (in red) and core (in blue) as a function of the forcing frequency ($A_m/A = 1/10$, $e_f = 1/10$, $e = 2/15$, and $\tilde{\phi} = 1$).

becomes infinite at the frequency

$$\omega_E = e, \tag{27}$$

which corresponds to the resonance with the well-known *Eulerian free wobble* of rigid-body dynamics (see, e.g., Landau & Lifshitz 1969). Equation (26) also corresponds to the solution of Equation (24) in the limit of $\tilde{m}_f = 0$. This is expected, as in this case the liquid core rotates uniformly with the mantle and the whole planet behaves as a solid body. The other limit $\tilde{m} = 0$ corresponds to the situation where the planet rotates steadily around the z-axis. In this case, we find that the liquid core must oscillate with frequency:

$$\omega_{som} = -(1 + e_f). \tag{28}$$

This is nothing other than the frequency of the SOM of a fluid inside a steadily rotating (oblate) ellipsoid. This frequency is not usually written as in Equation (28) (see, however, Smith 1977). In Appendix B we show that this expression is equivalent to the more usual formula derived from the momentum conservation equation of rotating fluid dynamics.

Using the definitions of Equations (27) and (28), we may rewrite Equation (24) as

$$\begin{pmatrix} \omega - \omega_E & (1+\omega)\dfrac{A_f}{A} \\ \omega & \omega - \omega_{som} \end{pmatrix} \begin{pmatrix} \tilde{m} \\ \tilde{m}_f \end{pmatrix} = \begin{pmatrix} e\tilde{\phi} \\ 0 \end{pmatrix}. \tag{29}$$

We find the free rotational modes by solving the above for $\tilde{\phi} = 0$. There are two independent eigenfrequencies corresponding to the roots of the characteristic polynomial:

$$\Delta \equiv (\omega - \omega_E)(\omega - \omega_{som}) - \omega(1+\omega)\frac{A_f}{A} = 0. \tag{30}$$

At this point, we remind the reader that the solutions to Equation (30)—based on Equation (15)—are only expected to be valid to first order in the flattening parameters e and e_f. To this order, the first solution is written as

$$\omega_{fcn} = -1 + \frac{A}{A_m}(1 + \omega_{som}) \tag{31}$$

$$= -1 - \frac{A}{A_m}e_f, \tag{32}$$

which we recognize as the frequency of the FCN, also known as the *nearly diurnal free wobble* (NDFW) owing to its proximity to the (retrograde) diurnal frequency in the mantle frame. This proximity makes it a very important mode in the study of nutations, as it tends to be greatly amplified by the TOM, a phenomenon that Poincaré (1910) described as a "double resonance." The second solution is written as

$$\omega_{cw} = \frac{A}{A_m}\omega_E \tag{33}$$

$$= \frac{A}{A_m}e, \tag{34}$$

which corresponds to the frequency of the mode known as the *Chandler wobble* (CW), named after the first astronomer to measure its frequency for Earth. This measured frequency is quite different from Equation (34) because of the combined effects of the mantle's elasticity—which are considered in Section 3.2 below—and surface processes (see, e.g., Rekier et al. 2022).

Finally, the general solution to Equation (29) may be written formally as

$$\begin{pmatrix} \widetilde{m} \\ \widetilde{m}_f \end{pmatrix} = \frac{A}{A_m}\frac{e\widetilde{\phi}}{(\omega - \omega_{fcn})(\omega - \omega_{cw})}\begin{pmatrix} \omega - \omega_{som} \\ -\omega \end{pmatrix}. \tag{35}$$

Interestingly, we see that $\tilde{m} = 0$ when $\omega = \omega_{som}$, something that can also be observed in Figure 1, showing the (normalized) kinetic energy of the mantle (in red) and the core (in blue) as measured in the SRF, for $A_m/A = 1/10$, $e_f = 1/10$, and $e = 2/15$, corresponding to a planet with a large (heavy) fluid core

and a comparatively small (light) mantle. We see that the kinetic energies of both the mantle and the core are infinite at the frequencies $\omega_{\rm fcn}$ and $\omega_{\rm cw}$, indicated by dashed lines, as expected from Equation (35), and that these also become infinite when $\omega = -1$, corresponding to the resonance with the TOM (see the next section). The kinetic energy of the mantle is zero at $\omega_{\rm som}$, indicated by the dotted line, whereas that of the core remains finite. The presence of a third resonance at $\omega = -1$ might seem counterintuitive. It comes from our choice to plot our results in the SRF, whose orientation with respect to the mantle frame is given by Equation (A9), which, when added to the system given by Equation (29), introduces the additional resonance corresponding to the TOM (see next section).

Another thing to mention is that although from Equation (35) it might seem that $\tilde{m}$ and $\tilde{m}$ become infinite at the resonances, this is never the case in practice, as nonlinear effects disregarded here start to be important before it happens. This is also true for the other results given below.

2.4. The Spin-over and Tilt-over Modes

The SOM is a free mode of the two-layer model's fluid core *only when the mantle*'s rotation is steady (Triana et al. 2019; Rekier et al. 2020). From Equation (35), we see that its frequency, $\omega_{\rm som}$, also corresponds to that where the amplitude of the mantle's motion is zero, $\tilde{m} = 0$. We can understand the reason for this by taking the ratio of the two components of the solution:

$$\tilde{m}_{\rm f} = -\frac{\omega\, \tilde{m}}{\omega - \omega_{\rm som}}. \tag{36}$$

Equation (36) can be arrived at by working directly from the momentum equation of fluid dynamics applied to the core flow (see Appendix B). This formula can also be obtained directly by considering the second row of Equation (29), which, in isolation, can be interpreted as describing the wobbly response of the liquid core, $\tilde{m}_{\rm f}$, subjected to a *prescribed* wobbly perturbation, $\tilde{m}$, at the forcing frequency, ω. When $\tilde{m}$ is constant, such perturbation corresponds to a steady precession of the mantle around the z-axis. In this case, it is a well-known fact that the flow response has a resonance at the SOM frequency, in agreement with Equation (36) (Poincaré 1910; Busse 1968; Noir & Cébron 2014).

By contrast, the fluid core wobble of a freely rotating planet remains finite when $\omega = \omega_{\rm som}$, as both numerator and denominator in Equation (36) become zero. Looking back at the equatorial projection of Equation (1) and setting $\tilde{\boldsymbol{m}} = 0$ there, we can see that this corresponds to the frequency where the torque produced on the mantle by the external potential is exactly balanced by that produced by the fluid core, leaving the mantle in a state of steady rotation.

The SOM frequency is close, although importantly not equal, to that of the TOM, even though the two names have sometimes been used interchangeably, as mentioned in the Introduction. Whereas the SOM owes its existence to that of the planet's fluid core, and its frequency depends on the core's flattening, the TOM exists for *all* rotating objects, regardless of their shape or internal structure, and its frequency is always *exactly* equal to $\omega = -1$. The TOM has already been described in detail by many authors (see, e.g., Smith 1977; Wahr 1981; Rogister 2001). In Appendix A, we show that this frequency is equal to zero when measured in the inertial frame, or equivalently that the associated motion has an infinite period, $T \to \infty$. If an external torque with such a period were to be applied on the planet, such as that produced on the spheroidal Earth's figure by a stationary object at a positive celestial latitude, it would respond by *tilting* its orientation in space permanently in the direction of the torque. When observed in the mantle frame, this reorientation corresponds to an exactly diurnal retrograde motion of the rotation axis around the planet's figure axis. The importance of this mode for the nutation can be understood by considering the dynamic relation between the wobble and the nutation amplitude given at the bottom of Appendix A.

2.5. Transfer Function

An important concept in the study of nutations is that of the *transfer function*, defined as the ratio of the wobble computed for the planetary model considered to the rigid wobble given by Equation (26):

$$T(\omega) \equiv \frac{\widetilde{m}(\omega)}{\widetilde{m}_R(\omega)} = \frac{\widetilde{\eta}(\omega + 1)}{\widetilde{\eta}_R(\omega + 1)}, \tag{37}$$

where T should not be confused with the period T. The second equality follows from Equation (A9) of Appendix A (see also Dehant & Mathews 2015b). This function allows us to separate the computation of nutations into two parts. In the first step, the nutations are computed from ephemerides for a hypothetical rigid planet with flattening e. The actual nutations can then be obtained for the more realistic planetary model as a second step by multiplication with $T(\omega)$ containing all the information on the planet's internal structure.

Incorporating the first component of Equation (35) into Equation (37), we obtain the expression for the transfer function of the two-layer model:

$$T(\omega) = \frac{A}{A_{\rm m}} \frac{(\omega - \omega_{\rm E})(\omega - \omega_{\rm som})}{(\omega - \omega_{\rm cw})(\omega - \omega_{\rm fcn})}. \tag{38}$$

This transfer function does not satisfy the gyrostatic rigidity condition exactly, which imposes that $T(-1) = 1$ (see Section 2.3, above). That is because the formalism used to arrive at Equation (38) is only valid to first order in the planet's flattening. This can be remedied by introducing the normalized transfer function:

$$\overline{T}(\omega) = \frac{A}{A_{\rm m}} \frac{(1 + \omega_{\rm cw})}{(1 + \omega_{\rm E})} \frac{(\omega - \omega_{\rm E})(\omega - \omega_{\rm som})}{(\omega - \omega_{\rm cw})(\omega - \omega_{\rm fcn})}, \tag{39}$$

which has all the right properties and also satisfies $\bar{T}(-1) = 1$ exactly. Figure 2 shows this normalized transfer function for the same parameters as Figure 1. Incidentally, note that gyrostatic rigidity prohibits making the approximation $e(\omega - \omega_{\rm som}) \approx e(\omega + 1)$ (which is the limit taken by, e.g., Dehant & Mathews 2015a) in the first component of Equation (35), even though this might seem to be the consistent choice to first order in e and $e_{\rm f}$. Finally, note that $T(\omega)$ is close to $\bar{T}(\omega)$ for all values of ω provided that

$$\omega_{\rm cw} - \omega_{\rm E} = \frac{A_{\rm f}}{A_{\rm m}} e \ll 1. \tag{40}$$

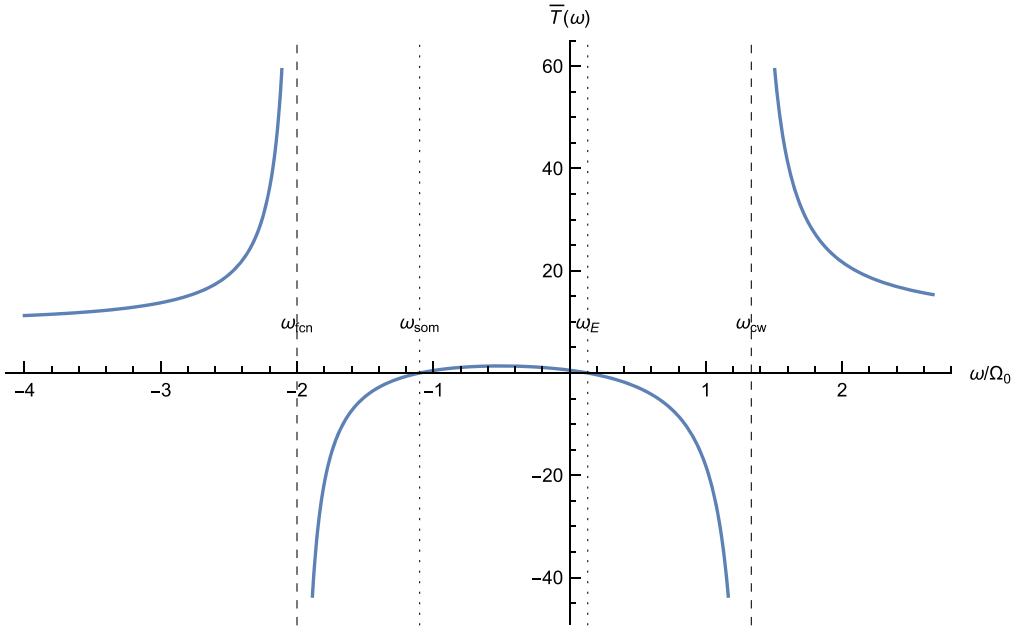

Figure 2. Normalized transfer function of a (rigid) two-layer planet with a large (heavy) liquid core and a comparatively small (light) mantle ($A_m/A = 1/10$, $e_f = 1/10$, and $e = 2/15$).

Table 1
Ratio of the Equatorial Moments of Inertia, Dynamical Flattenings, Compliance Parameters, and CMB Coupling Constant for Earth (Dehant & Mathews 2015b; Zhu et al. 2017)

Symbol	A_m/A	$e \times 10^3$	$e_f \times 10^3$	$\kappa \times 10^3$	$\xi \times 10^3$	$\beta \times 10^3$	$\gamma \times 10^3$	$K_{cmb} \times 10^3$
Earth	0.887	3.285	2.548	1.039	0.222	0.616	1.965	$0.128 - i0.019$

This is true in most planetary applications where e is small, and the inertia of the mantle is much bigger than the core's. For example, in Earth, $A_f/A_m \approx 1/9$ (see Table 1).

The expression of the transfer function in Equation (38) (or Equation (39)) is quite satisfying. Its *zeros*, ω_E and ω_{som}, respectively correspond to the free modes of oscillations of the mantle and the core taken in isolation, i.e., of the freely rotating mantle shell with a hollow center (for which $A_f = 0$) and the steadily rotating fluid core (for which $A_m \to \infty$). On the other hand, its *poles*, ω_{cw} and ω_{fcn}, correspond to the two rotational modes of the fully coupled freely rotating two-layer system. It should be noted, however, that although the two roots, ω_E, and ω_{som}, are treated on the same footing in Equation (38), they have a somewhat different physical interpretation: the former ensures that the amplitude of the nonrigid wobble remains finite when $\omega = \omega_E$, whereas the latter introduces a "true" zero, as is clearly visible from Figure 1. This zero can have a detectable effect on the amplitudes of the FCN and nutation amplitudes in Earth and other planets, as will be discussed in the next section.

3. Application to Earth

3.1. Rigid Mantle

In the example of the previous section, we have used values of the parameters that are quite different from those found in planetary applications. This was done in order to accentuate the differences between ω_{fcn} and ω_{som}, on the one hand, and between ω_{cw} and ω_E, on the other. In particular, we had $A_m < A_f$, whereas, as we have already mentioned, the opposite is true in most cases. In addition, the values of e and e_f for real planets are typically one order of magnitude smaller than those we have used. Figure 3 shows the normalized kinetic energy of the mantle (in red) and core (in blue), similarly to Figure 1 for values of the parameters closer to those found in Earth ($A_m/A = 9/10$, $e_f = 1/400$, $e = 1/300$, and $\tilde{\phi} = 1$). The top panel is centered around ω_{fcn}, and the bottom panel around ω_{cw}. The values of ω_{fcn} and ω_{som} are so close in this case that it is easier to compare their periods (in days) as measured in the inertial frame of reference based on the following formula (see Dehant et al. 2017 and Appendix A):

$$T_{inertial} = (\Omega_0 + \omega)^{-1}. \quad (41)$$

Accordingly, the period of the TOM, visible on the right edge of the figure, is infinite. On the other hand, the period of the CW is more readable in the rotating frame (SRF) according to the following formula:

$$T_{srf} = \omega^{-1}. \quad (42)$$

One important difference compared to the example of Figure 1 is that the kinetic energy of the core is larger than that of the mantle in the vicinity of $\omega = \omega_{fcn}$ (they are both infinite at that precise frequency). This is consistent with the traditional interpretation of the FCN as a core motion, which is reflected in its name. What this study shows is that this is even more true at $\omega = \omega_{som}$, where the mantle is immobile. The opposite situation is true in the vicinity of $\omega = \omega_{cw}$, where the kinetic energy of the mantle dominates over that of the core. The numerical values of $T_{fcn} = -360$ days in the inertial frame and $T_{cw} = 270$ days in the rotating frame are quite different from those

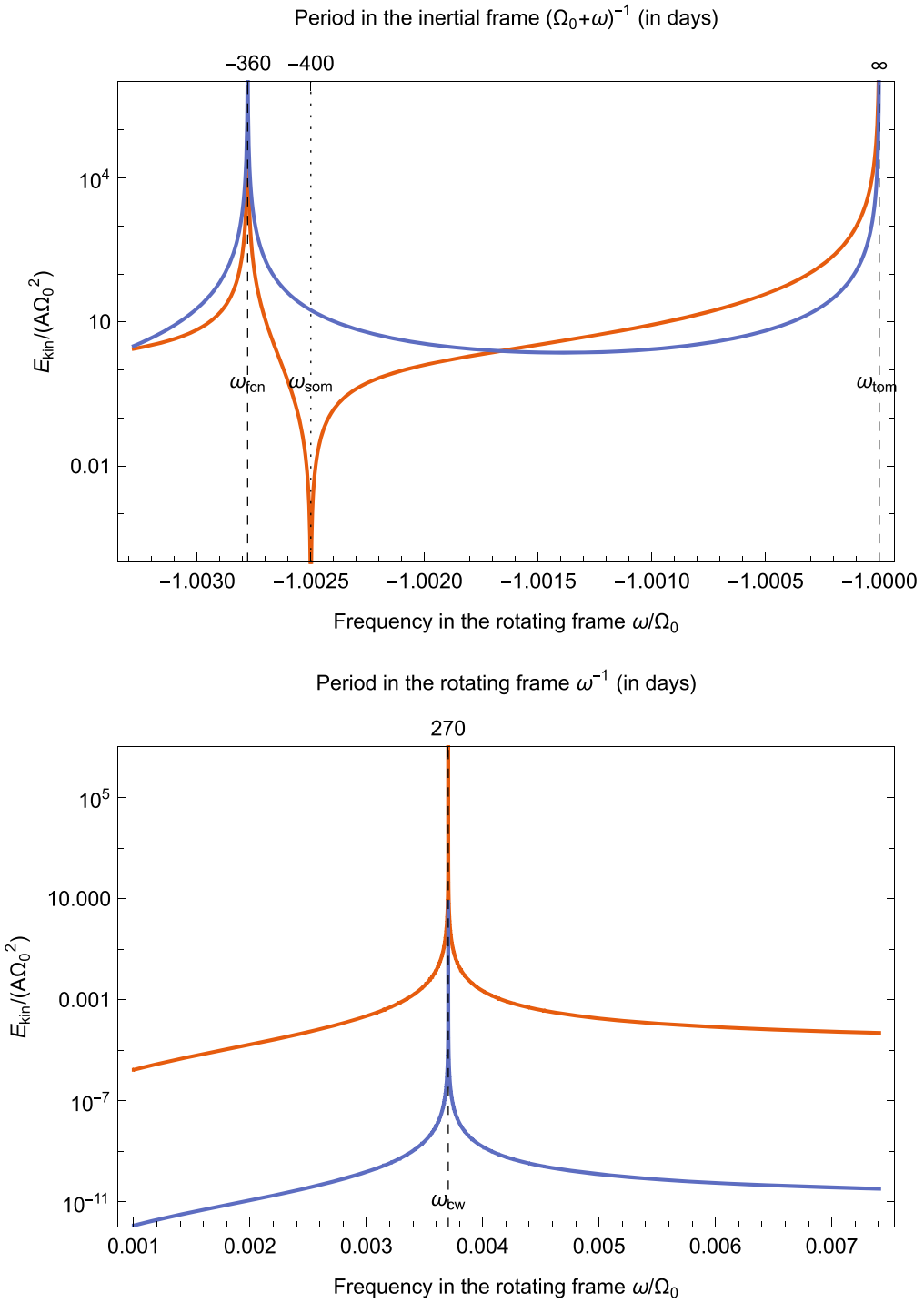

Figure 3. Normalized kinetic energy of the mantle (in red) and core (in blue) as a function of the forcing frequency ($A_m/A = 9/10$, $e_f = 1/400$, $e = 1/300$, and $\tilde{\phi} = 1$). Top: centered around ω_{fcn}. Bottom: centered around ω_{cw}.

measured for the real Earth, where elasticity plays an important role in lengthening the periods of those modes, as we now discuss.

3.2. Elastic Mantle

Real planets are never perfectly rigid; they deform under the effects of gravity and internal pressure forces. In the case of a hypothetical single-layer planet, elasticity can be shown to shorten the Eulerian frequency to (Munk & MacDonald 1960)

$$\bar{\omega}_E \approx \omega_E\left(1 - \frac{k_2}{k_s}\right), \tag{43}$$

where k_2 and $k_s = 3eGA/(\Omega_0^2 R^5) > k_2$ denote the degree-2 elastic and secular Love numbers, respectively, and where G and R are the gravitational constant and the mean planetary radius, respectively. Because of the accidental proximity between Equation (43) and the measured CW frequency for

Earth, $\bar{\omega}_{\rm E}$ has sometimes been identified with that mode. In reality, the CW frequency of the real Earth is altered by the oceans present at its surface (Smith & Dahlen 1981; Wahr 1984), and by the existence of the fluid core (Dehant & Mathews 2015b; see also below).

The effects of elasticity on planetary rotation can be incorporated in models through the use of *compliance parameters* measuring the changes in the tensor of inertia of the planet and its fluid core, $\Delta\underline{\boldsymbol{I}}$ and $\Delta\underline{\boldsymbol{I}}_{\rm f}$. To leading order, in the wobble it can be shown that one need only consider the two combinations, $\widetilde{\Delta I} \equiv (\Delta I^{xz} + i\Delta I^{yz})$ and $\widetilde{\Delta I}_{\rm f} \equiv (\Delta I_{\rm f}^{xz} + i\Delta I_{\rm f}^{yz})$. Following Sasao et al. (1980), these may then be parameterized as

$$\widetilde{\Delta I} = A\,[\kappa(\tilde{m} - \tilde{\phi}) + \xi\tilde{m}_{\rm f}], \tag{44}$$

$$\widetilde{\Delta I}_{\rm f} = A_{\rm f}[\gamma(\tilde{m} - \tilde{\phi}) + \beta\tilde{m}_{\rm f}], \tag{45}$$

where κ, ξ, γ, and β are the four compliance parameters.

Remarkably, Sasao et al. have shown that their Equation (15) remains valid to the same order of approximation provided that the compliance parameters are of the same order as the dynamical flattenings, e and $e_{\rm f}$, which is typically the case in all planetary applications. Upon using Equations (44) and (45), Equation (24) is now replaced by (Mathews et al. 1991)

$$\begin{pmatrix} \omega - e + \kappa(1+\omega) & (1+\omega)\left(\dfrac{A_{\rm f}}{A} + \xi\right) \\ (1+\gamma)\omega & (1+\beta)\omega + (1+e_{\rm f}) \end{pmatrix} \begin{pmatrix} \tilde{m} \\ \tilde{m}_{\rm f} \end{pmatrix} = \tilde{\phi}\begin{pmatrix} e - \kappa(1+\omega) \\ -\gamma\omega \end{pmatrix}. \tag{46}$$

Importantly, by incorporating $\omega = -1$ into Equation (46), we see that the elastic two-layer system satisfies the gyrostatic rigidity constraint.

By analogy with Section 2.3, we define the SOM of the steadily rotating two-layer elastic planet as the solution of Equation (46) for $\tilde{m} = \tilde{\phi} = 0$. This gives the frequency

$$\bar{\omega}_{\rm som} = -\frac{1+e_{\rm f}}{1+\beta} \tag{47}$$

$$\approx \omega_{\rm som} + \beta. \tag{48}$$

Since $\beta > 0$ and $\omega_{\rm som} < 0$, we have $|\bar{\omega}_{\rm som}| < |\omega_{\rm som}|$. As expected, we see that elasticity shortens the SOM frequency, similarly to the Eulerian wobble.

The free mode frequencies of the coupled system are the roots of the characteristic polynomials of the matrix in Equation (46), which, upon using the above definitions for $\bar{\omega}_{\rm E}$ and $\bar{\omega}_{\rm som}$, may be written as

$$\Delta = (\omega - \bar{\omega}_{\rm E})(\omega - \bar{\omega}_{\rm som}) - \frac{(1+\gamma)}{(1+\beta)(1+\kappa)}\left(\frac{A_{\rm f}}{A} + \xi\right)\omega(1+\omega) = 0. \tag{49}$$

To first order in the dynamical flattening and compliance parameters, the two solutions corresponding to the "elastic" FCN and CW are respectively (e.g., Mathews et al. 1991, 2002)

$$\bar{\omega}_{\rm fcn} = -1 - \frac{A}{A_m}(e_{\rm f} - \beta), \tag{50}$$

$$\bar{\omega}_{\rm cw} = \frac{A}{A_m}(e - \kappa). \tag{51}$$

Finally, to the same order, the solution to Equation (46) can be written as

$$\tilde{m} = \frac{A}{A_m}\frac{(e - (1+\omega)\kappa + \epsilon\omega)}{(\omega - \bar{\omega}_{\rm fcn})(\omega - \bar{\omega}_{\rm cw})}\left(\omega - \frac{e\bar{\omega}_{\rm som} + \epsilon}{e - \epsilon}\right)\tilde{\phi}, \tag{52}$$

$$\tilde{m}_{\rm f} = -\frac{A}{A_m}\frac{(e - (1+\omega)\kappa + \gamma\omega)}{(\omega - \bar{\omega}_{\rm fcn})(\omega - \bar{\omega}_{\rm cw})}\omega\tilde{\phi}, \tag{53}$$

where we have introduced the following new parameter:

$$\epsilon = \frac{A_{\rm f}}{A}\gamma, \tag{54}$$

which satisfies $0 < \epsilon < \gamma$. We see that, contrary to what we might have guessed from the rigid case, $\tilde{m}$ is not zero at $\omega = \bar{\omega}_{\rm som}$, but rather at another frequency equal to

$$\bar{\omega}_{\rm som}^{\epsilon} \equiv \frac{e\bar{\omega}_{\rm som} + \epsilon}{e - \epsilon} \lessapprox \bar{\omega}_{\rm som}. \tag{55}$$

We can understand this result by realizing that any given flow inside the core produces a torque on the elastic mantle, thereby changing its moments of inertia. Equation (55) gives the forcing frequency at which this change exactly balances the additional momentum. When the moment of inertia of the mantle is much bigger than the fluid's, corresponding to the limit $A_{\rm f}/A \to 0$, then $\epsilon \to 0$, and $\bar{\omega}_{\rm som}^{\epsilon} \to \bar{\omega}_{\rm som}$. The variable $\omega_{\rm som}^{\epsilon}$—where ϵ should not be confused with an exponent—is chosen to acknowledge its relation with the SOM.

Elasticity also introduces two new roots in $\tilde{m}$ and $\tilde{m}_{\rm f}$ at $\omega = (e - \kappa)/(\kappa - \epsilon)$, and $\omega = (e - \kappa)/(\kappa - \gamma)$, respectively. These correspond to the frequencies at which the total torque acting on the whole planet or on the fluid core, respectively, is exactly balanced by a change in their inertia tensors. This is something that is not possible for a rigid mantle.

Figure 4 shows the normalized kinetic energy of the mantle (in red) and fluid core (in blue) in the SRF for an elastic two-layer planet resembling Earth, with values of the parameters given in Table 1. A somewhat surprising feature of this figure is the fact that there is not just one but two frequencies at which the kinetic energy of the fluid core is zero (indicated by dotted lines), and neither of these corresponds to the value of $\omega = (e - \kappa)/(\kappa - \gamma)$ derived above. The reason for this is that the total kinetic energy of the fluid core in the SRF is proportional to the square of the sum of the angular velocities of the core and mantle (see Equation (12)). The kinetic energy of the core is therefore zero when those two vectors add up to zero. The expressions of the two values of the forcing frequency, ω_0, where this balance takes place are quite long and not very informative. However, they can be shown to satisfy

$$\tilde{m}_{\rm f}(\omega_0) = -\frac{\omega_0\tilde{m}(\omega_0)}{\omega_0 + 1}. \tag{56}$$

This circumstance is unique to the elastic two-layer model and does not exist in the rigid model where $\tilde{m}$ and $\tilde{m}$ satisfy Equation (36) for all values of ω, which is incompatible with Equation (56), except in the trivial (spherical) limit where $\omega_{\rm som} \to -1$. Note that, for the parameters of Table 1, the difference between the values of $\bar{\omega}_{\rm som}$ and $\bar{\omega}_{\rm som}^{\epsilon}$—though small—corresponds to a nonnegligible difference of period

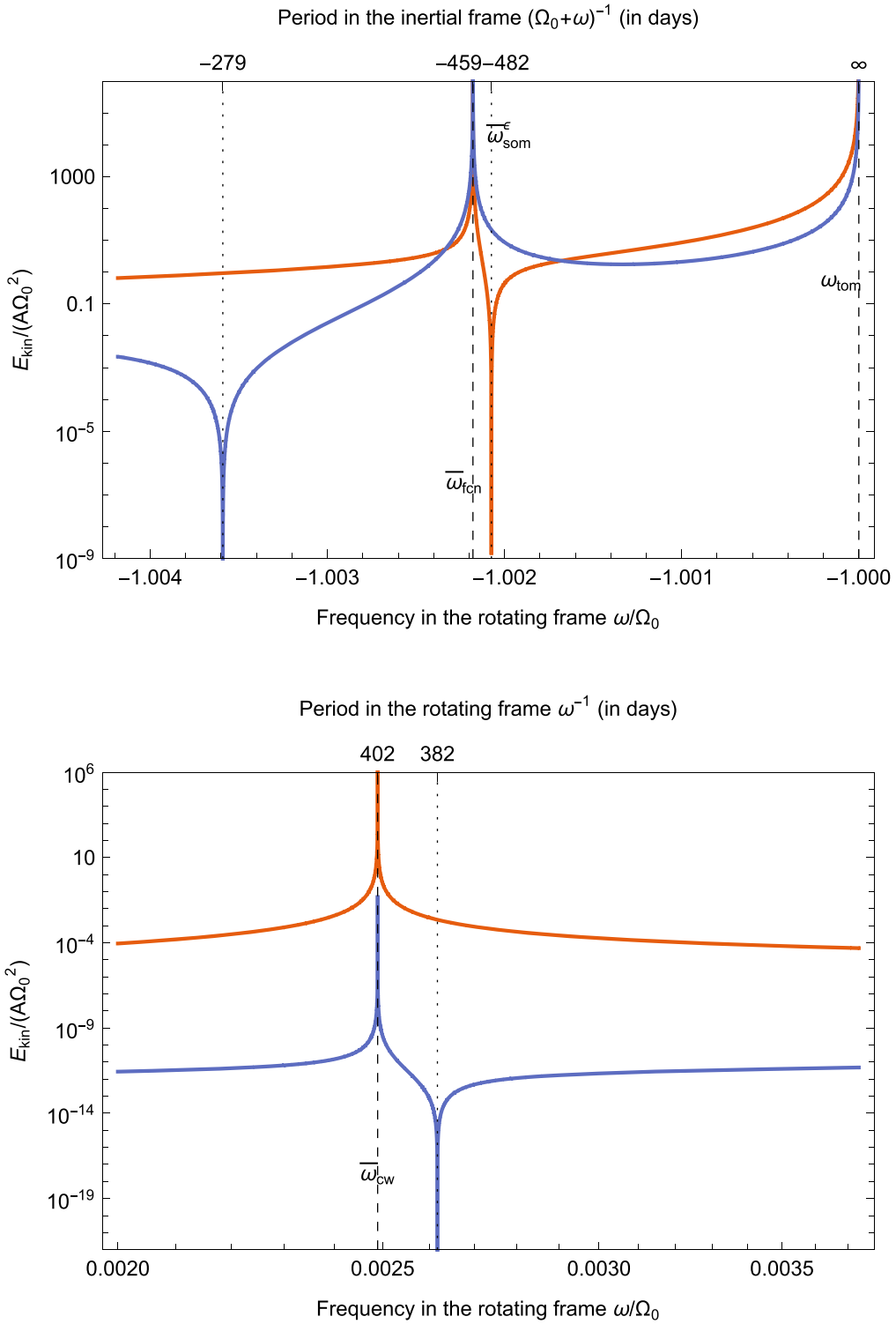

Figure 4. Normalized kinetic energy of the mantle (in red) and core (in blue) for the two-layer elastic planet as a function of the forcing frequency ($\tilde{\phi} = 1$, other parameters are given in Table 1). Top: centered around $\bar{\omega}_{\rm fcn}$. Bottom: centered around $\bar{\omega}_{\rm cw}$.

of ≈ -35 days measured in the inertial frame, bringing $\bar{\omega}^{\epsilon}_{\rm som}$ closer to the value of $\bar{\omega}_{\rm fcn}$.

3.3. Additional Coupling at the CMB

In addition to the gravitational and pressure torques that are accounted for in Equation (15), there are other torques at the CMB contributing to the exchange of angular momentum between the core and mantle. It is customary to parameterize those extra torques by introducing a single parameter, $\mathbf{\Gamma}_{\rm cmb}$, into the right-hand side of Equation (15):

$$\frac{d\boldsymbol{H}_{\rm f}}{dt} - \boldsymbol{\omega}_{\rm f} \times \boldsymbol{H}_{\rm f} = \mathbf{\Gamma}_{\rm cmb}. \tag{57}$$

This most notably includes the *electromagnetic torque* produced by the induced electric currents at the base of the

mantle (Buffett 1992; Buffett et al. 2002; Dumberry & Koot 2012), combined with the *viscous torque* caused by the frictions between the mantle and the viscous fluid core (Mathews & Guo 2005; Deleplace & Cardin 2006; Koot et al. 2010). The computation of the exact dependence of $\mathbf{\Gamma}_{\rm cmb}$ on those two physical phenomena and others is highly nontrivial. For simplicity, it is customary to use the following parameterization attributed to Sasao et al. (1980):

$$\mathbf{\Gamma}_{\rm cmb} = -\Omega_0 A_{\rm f}(K_1\hat{\boldsymbol{z}} \times (\boldsymbol{\omega}_{\rm f} - \boldsymbol{\omega}_{\rm f}^{\parallel}) - K_2(\boldsymbol{\omega}_{\rm f} - \boldsymbol{\omega}_{\rm f}^{\parallel}) - K_3\boldsymbol{\omega}_{\rm f}^{\parallel}), \tag{58}$$

where $\boldsymbol{\omega}_{\rm f}^{\parallel} \equiv (\boldsymbol{\omega}_{\rm f}\cdot\hat{\boldsymbol{z}})\hat{\boldsymbol{z}}$ is the axial part of $\boldsymbol{\omega}_{\rm f}$, and where K_1, K_2, and K_3 are real-valued *coupling constants*. Equation (58) is similar in shape to the formulae given by Noir et al. (2003) and Noir & Cébron (2014) based on the work of Busse (1968) for the viscous torque of a fluid on an ellipsoidal boundary. The first term in this equation accounts for the torque exerted by the mantle on the fluid core by viscous and electromagnetic—and possibly other—forces. The second term accounts for the *power dissipated* by those forces. The third term of Equation (58) only affects the planet's spin rate and has no effect on the wobble, as can be seen by combining the two equatorial components of $\mathbf{\Gamma}_{\rm cmb}$ in the usual fashion to yield

$$\widetilde{\Gamma}_{\rm cmb} = -iK_{\rm cmb}\Omega_0^2 A_{\rm f}\widetilde{m}_{\rm f}, \tag{59}$$

where we have defined

$$K_{\rm cmb} \equiv K_1 + iK_2. \tag{60}$$

The values of K_1 and K_2 are typically of the same order of magnitude as e, $e_{\rm f}$, and the compliance parameters in planetary applications (see Table 1). We should emphasize that the torque given by Equation (58) is *not* equivalent to having $\mathbf{\Gamma}_{\rm cmb} \sim K_{\rm cmb}\boldsymbol{\omega}_{\rm f}$, contrary to what one might guess by working directly from Equation (59).

Introducing Equation (59) into Equation (57), the dynamical equations for the elastic two-layer planet then become

$$\begin{pmatrix} \omega - e + \kappa(1+\omega) & (1+\omega)\left(\dfrac{A_{\rm f}}{A} + \xi\right) \\ (1+\gamma)\omega & (1+\beta)\omega + (1 + e_{\rm f} + K_{\rm cmb}) \end{pmatrix}\begin{pmatrix}\widetilde{m} \\ \widetilde{m}_{\rm f}\end{pmatrix} = \widetilde{\phi}\begin{pmatrix} e - \kappa(1+\omega) \\ -\gamma\omega \end{pmatrix}. \tag{61}$$

Notice that $K_{\rm cmb}$ only appears in the second row of the matrix. By inspection of Equation (61), we immediately obtain the frequency of the SOM in the coupled case:

$$\begin{aligned}\bar{\omega}_{\rm som} &= -\frac{1 + e_{\rm f} + K_{\rm cmb}}{1+\beta} \\ &\approx \omega_{\rm som} + \beta - K_{\rm cmb}.\end{aligned} \tag{62}$$

Similarly, the frequency of the FCN now reads (Sasao et al. 1980; Dehant & Mathews 2015b)

$$\bar{\omega}_{\rm fcn} = -1 - \frac{A}{A_{\rm m}}(e_{\rm f} + K_{\rm cmb} - \beta). \tag{63}$$

Importantly, $\bar{\omega}_{\rm cw}$ remains the same to this order of approximation, reflecting the fact that this mode is only weakly affected by $\mathbf{\Gamma}_{\rm cmb}$ compared to the FCN. The solutions given by Equations (52) and (53) remain valid, provided that one uses $\bar{\omega}_{\rm som}$ and $\bar{\omega}_{\rm fcn}$ defined by Equations (62) and (63).

3.4. Transfer Function

The fact that $K_{\rm cmb}$ is a complex number introduces qualitative changes to the dynamics of the two-layer model besides the quantitative shifts in the values of $\bar{\omega}_{\rm som}$ and $\bar{\omega}_{\rm fcn}$. These can be appreciated by looking at the—now complex-transfer function, whose amplitude and phase are shown in the top and bottom panels of Figure 5, respectively. The yellow curve corresponds to the parameters of Table 1, and the blue curve is the same thing but for $K_{\rm cmb} = 0$. To facilitate comparison, we have adjusted the value of $e_{\rm f}$ so that the numerical values of both $\bar{\omega}_{\rm fcn}$ and $\bar{\omega}_{\rm som}$ are the same in both curves. This amounts to treating the combination $e_{\rm f} + {\rm Re}(K_{\rm cmb})$ as a constant, which corresponds to what is actually measured in observations (see Dehant et al. 2017; Zhu et al. 2017). In order to emphasize the role of $\bar{\omega}_{\rm som}^{\epsilon}$, we have also added the green curve, which is similar to the yellow one but with the substitution $\bar{\omega}_{\rm som}^{\epsilon} \to -1$ in Equation (52). This corresponds to the naive limit, which we have already shown to be incompatible with the gyrostatic rigidity constraint in Section 2.5, and is here considered only for illustrative purposes.

There are two things to observe from the top panel. First, by comparing the yellow and green curves to the blue one, we see that having ${\rm Im}(K_{\rm cmb}) \neq 0$ causes the magnitude of the transfer function to remain finite for all values of the frequencies, even near the pole at $\bar{\omega}_{\rm fcn}$. Something similar can be observed near $\bar{\omega}_{\rm som}^{\epsilon}$, where the yellow curve never reaches zero, contrary to the blue one. This is the expected behavior for dynamics systems described by a transfer function with complex zeros and/or poles (see, e.g., Franklin et al. 1994). Second, we can see that the maximum of the yellow curve is considerably smaller and that it is slightly offset to the left compared to the green one, corresponding to a period of ≈ -1 day in the inertial frame. As the two curves correspond to exactly the same coupling at the CMB, it is clear that this difference cannot by explained by the presence of dissipation alone. In the next section, we show that both of these observations can be interpreted as a consequence of the proximity between the numerical values of $\bar{\omega}_{\rm fcn}$ and $\bar{\omega}_{\rm som}^{\epsilon}$. This can already by appreciated by looking at the bottom panel, which shows that this proximity prevents a complete phase reversal of the yellow curve, contrary to the green one. Another more subtle effect of this proximity is to slightly widen the peak in the yellow curve. This can be measured from the *quality factor*, Q, defined as

$$Q = \left|\frac{\omega_{\rm max}}{\Delta\omega}\right|, \tag{64}$$

where $\omega_{\rm max}$ is the frequency at resonance and $\Delta\omega$ is the width of that resonance defined as the difference between the two values of ω for which $|T(\omega)| = |T(\omega_{\rm max})|/\sqrt{2}$. This last quantity is shown as the red double arrow in Figure 5. For the yellow curve we find $Q_{\rm fcn} \approx 22,000$, which is slightly lower than for the green curve ($Q_{\rm fcn} \approx 24,000$).

4. Discussion

4.1. Offset in the FCN Resonance Frequency

In the previous section, we have shown how the existence of dissipation at the CMB causes a slight offset of the maximum in the magnitude of the transfer function compared to the FCN

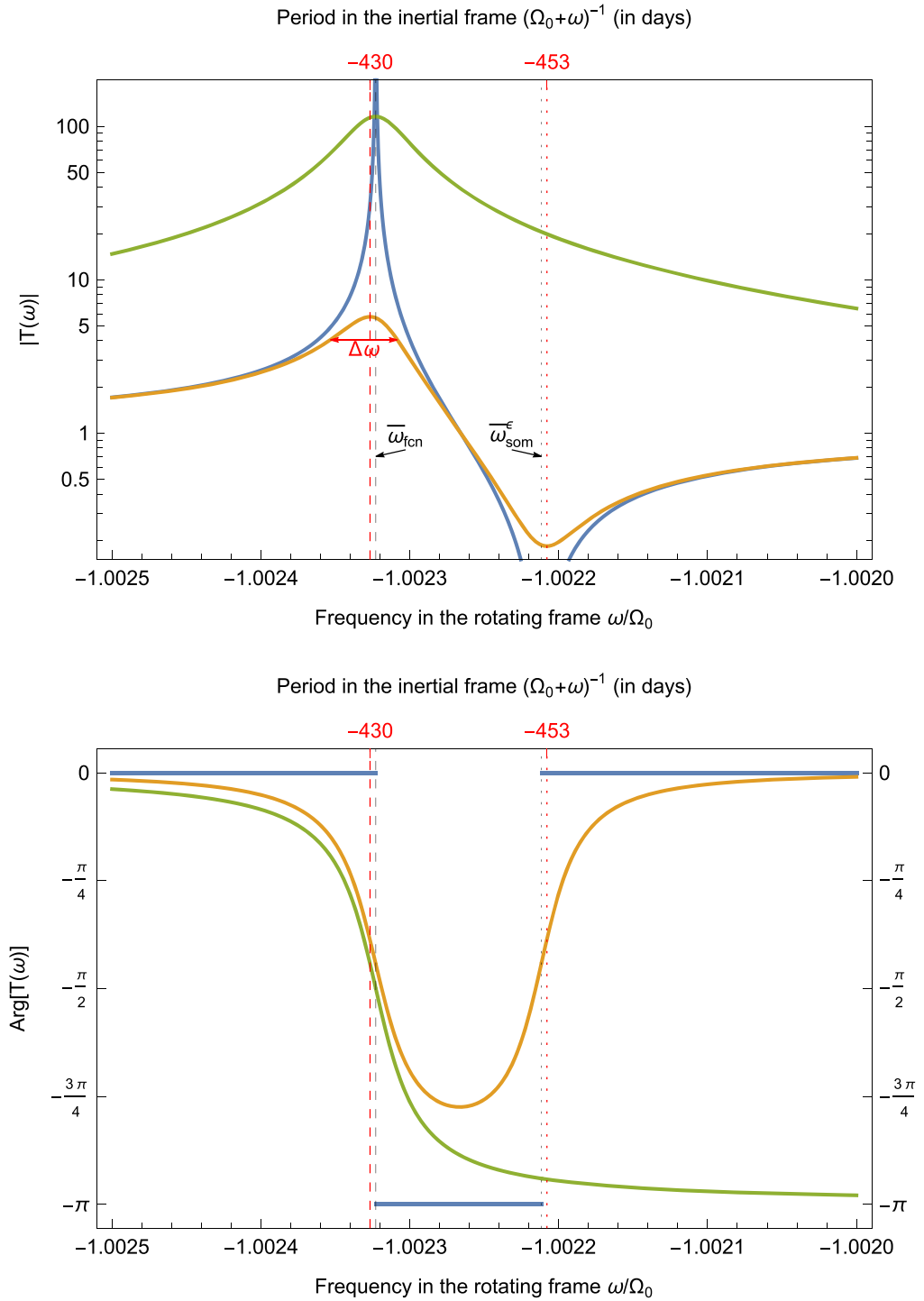

Figure 5. Magnitude (top) and phase (bottom) of the transfer function for the two-layer elastic planet for the parameters of Table 1, with the exception that $e_{\rm f} + {\rm Re}(K_{\rm cmb})$ is treated as a constant (see main text). The blue curve corresponds to $K_{\rm cmb} = 0$, the yellow one to $K_{\rm cmb} \neq 0$, and the green one is similar to the yellow one but for $\bar{\omega}^{\epsilon}_{\rm som} \to -1$. The black dashed and dotted lines indicate the positions of the frequencies ${\rm Re}(\bar{\omega}_{\rm fcn})$ and ${\rm Re}(\bar{\omega}^{\epsilon}_{\rm som})$, respectively. Their red equivalents respectively correspond to the maximum and minimum of the yellow curve.

frequency. This is a well-known phenomenon that is commonly described by analogy with the simpler system of a single damped harmonic oscillator. The response of this system to excitation can be represented by a transfer function with a single pole and no zero. If we call ω_0, the free complex frequency of that system, one can then show that the damped resonance frequency, ω_d, and quality factor are equal to (Franklin et al. 1994, p. 122)

$$\omega_d = {\rm Re}(\omega_0)\sqrt{1 - \frac{{\rm Im}(\omega_0)^2}{{\rm Re}(\omega_0)^2}}, \; Q = \left| \frac{{\rm Re}(\omega_0)}{2\,{\rm Im}(\omega_0)} \right|. \tag{65}$$

Applying the above to Earth's, by setting $\omega_0 = \bar{\omega}_{\rm fcn}$ and using the fact that $|\,{\rm Im}(\bar{\omega}_{\rm fcn})| \ll |\,{\rm Re}(\bar{\omega}_{\rm fcn})| \approx 1$, we find

$$\omega_{\rm max} \approx {\rm Re}(\bar{\omega}_{\rm fcn}) - \frac{{\rm Im}\,(\bar{\omega}_{\rm fcn})^2}{2}. \tag{66}$$

This corresponds to a period shift of ≈ -3 s, much smaller than that computed in Section 3.4. For the quality factor, we find $Q \approx 24{,}000$. These two values are in agreement with those inferred from Figure 5 for the green curve, but not the yellow one. Since the difference between these two curves lies only in the value of $\omega^{\epsilon}_{\rm som}$ used, we deduce that the simple harmonic oscillator analogy works well only in the case when the values of $\omega_{\rm fcn}$ and $\omega^{\epsilon}_{\rm som}$ are not too close to each other. We can make this statement a little more precise if we define

$$\delta \equiv \bar{\omega}_{\rm fcn} - \bar{\omega}^{\epsilon}_{\rm som}. \tag{67}$$

One can then show that the magnitude of the transfer function is maximum at

$$\omega_{\rm max} = {\rm Re}(\bar{\omega}_{\rm fcn}) - \frac{{\rm Re}(\delta)}{2} \times \left(1 + \frac{{\rm Im}\,(\delta)^2}{{\rm Re}\,(\delta)^2} - \frac{{\rm Im}(\delta){\rm Im}(\bar{\omega}_{\rm fcn})}{{\rm Re}\,(\delta)^2}\right) + \frac{|\delta|}{2}\sqrt{1 + \left(\frac{{\rm Im}(\delta) - 2\,{\rm Im}(\bar{\omega}_{\rm fcn})}{{\rm Re}(\delta)}\right)^2}. \tag{68}$$

The same function is minimum at the frequency

$$\omega_{\rm min} = {\rm Re}(\bar{\omega}_{\rm fcn}) - \frac{{\rm Re}(\delta)}{2} \times \left(1 + \frac{{\rm Im}\,(\delta)^2}{{\rm Re}\,(\delta)^2} - \frac{{\rm Im}(\delta){\rm Im}(\bar{\omega}_{\rm fcn})}{{\rm Re}\,(\delta)^2}\right) - \frac{|\delta|}{2}\sqrt{1 + \left(\frac{{\rm Im}(\delta) - 2\,{\rm Im}(\bar{\omega}_{\rm fcn})}{{\rm Re}(\delta)}\right)^2}. \tag{69}$$

These expressions are particularly enlightening in the limit $\delta \to 0$, where they converge to

$$\omega_{\rm max} \to {\rm Re}(\bar{\omega}_{\rm fcn}) - |\,{\rm Im}(\bar{\omega}_{\rm fcn})|, \tag{70}$$

$$\omega_{\rm min} \to {\rm Re}(\bar{\omega}_{\rm fcn}) + |\,{\rm Im}(\bar{\omega}_{\rm fcn})|. \tag{71}$$

Equation (70) shows that when the FCN and SOM frequencies are very close, the offset produced on the resonance frequency is linear in the quantity $|\,{\rm Im}(\bar{\omega}_{\rm fcn})|$ representing the mode's damping. This is in contrast with the result of Equation (66) for the simple harmonics oscillator, where this offset is quadratic. The fact that the simple model fails to predict the correct resonance frequency should not be a surprise given the superior complexity of the two-layer nutation model with dissipation. What the above computation shows is that this difference in behavior can be interpreted mathematically as the result of having a complex zero at a frequency close to that of the FCN in the system's transfer function. Similar behaviors can be found in other physical systems described by transfer functions (see again Franklin et al. 1994). The fact that in the present case the zero's frequency corresponds to $\bar{\omega}^{\epsilon}_{\rm som}$ is also interesting.

Despite their proven limitations, Equations (65) are commonly used in the literature to identify the frequency and quality factor of the FCN from the observations of its resonance with the nutations (e.g. Koot et al. 2010; Chao & Hsieh 2015) . In the following subsection, we reformulate the main elements of the above in the standard formalism in order to facilitate comparison with other works.

4.2. Comparison to Previous Work

In order to compare observations to theory, Mathews et al. (2002) introduced the following parameterization of the transfer function of an elastic planet with dissipation:

$$T(\omega) = \frac{\omega_{\rm E} - \omega}{1 + \omega_{\rm E}}\left(1 + (1 + \omega)\sum_{\alpha=1}\frac{N_\alpha}{\omega - \omega_\alpha}\right), \tag{72}$$

where the sum runs over the set of free modes with frequencies ω_α. There are two such modes in the two-layer system: the FCN and the CW. For a three-layer planet with a solid inner core, such as Earth, one must add to this list the *free inner core nutation* (FICN) and the *inner core wobble* (ICW). However, these two modes only have a small influence on the nutations compared to the FCN and CW and may therefore be excluded from the analysis in first approximation. The transfer function given by Equation (72) satisfies the gyrostatic rigidity constraint: $T(-1) = 1$, as well as $T(\omega_{\rm E}) = 0$. We can compute the expressions of the coefficients N_α analytically by direct comparison to the (normalized) transfer function of previous sections:

$$N_{\rm cw} = -\frac{A}{A_{\rm m}}\left(1 - \frac{\kappa}{e} + \frac{\epsilon - \kappa}{e}\bar{\omega}_{\rm cw}\right)\frac{(\bar{\omega}_{\rm cw} - \bar{\omega}^{\epsilon}_{\rm som})}{(\bar{\omega}_{\rm cw} - \bar{\omega}_{\rm fcn})}, \tag{73}$$

$$N_{\rm fcn} = -\frac{A}{A_{\rm m}}\left(1 - \frac{\kappa}{e} + \frac{\epsilon - \kappa}{e}\bar{\omega}_{\rm fcn}\right) \frac{(\bar{\omega}_{\rm fcn} - \bar{\omega}^{\epsilon}_{\rm som})}{(\bar{\omega}_{\rm cw} - \bar{\omega}_{\rm fcn})}\frac{(1 + \bar{\omega}_{\rm cw})}{(1 + \bar{\omega}_{\rm fcn})}. \tag{74}$$

To leading order in the small quantities, Equations (73) and (74) reduce to

$$N_{\rm cw} \approx -\frac{A}{A_{\rm m}}\left(1 - \frac{\kappa}{e}\right) = -\frac{\bar{\omega}_{\rm cw}}{e}, \tag{75}$$

$$N_{\rm fcn} \approx \frac{A_{\rm f}}{A_{\rm m}}\left(1 - \frac{\gamma}{e}\right), \tag{76}$$

in agreement with Mathews et al. (2002). As stated by these authors, direct measurements of the strengths and locations of the resonances in the amplitude of the nutations can then be used to constrain the parameters that appear in the explicit expressions for $\bar{\omega}_{\rm fcn}$, $\bar{\omega}_{\rm cw}$, and $N_{\rm fcn}$. The transfer function obtained from the values of Equations (75) and (76) is indistinguishable from that of Figure 5 (yellow curve). However, as we have shown in the previous subsection, caution must be exerted in identifying the frequency of the resonance with the FCN.

Using Equation (76), we can rewrite Equation (67) as

$$\delta = \left(-\frac{A_{\rm f}}{A_{\rm m}} + \frac{\epsilon}{e - \epsilon}\right)(e_{\rm f} - \beta + K_{\rm cmb}) \tag{77}$$

$$\approx \frac{N_{\rm fcn}}{1 + N_{\rm fcn}}(1 + \bar{\omega}_{\rm fcn}). \tag{78}$$

From Equation (74) we can see clearly that, in addition to causing the frequency offset computed in the previous section, having δ small also causes the decrease in the amplitude of the resonance. This is another expected effect of having a pole close to a zero in the transfer function (see again Franklin et al. 1994,

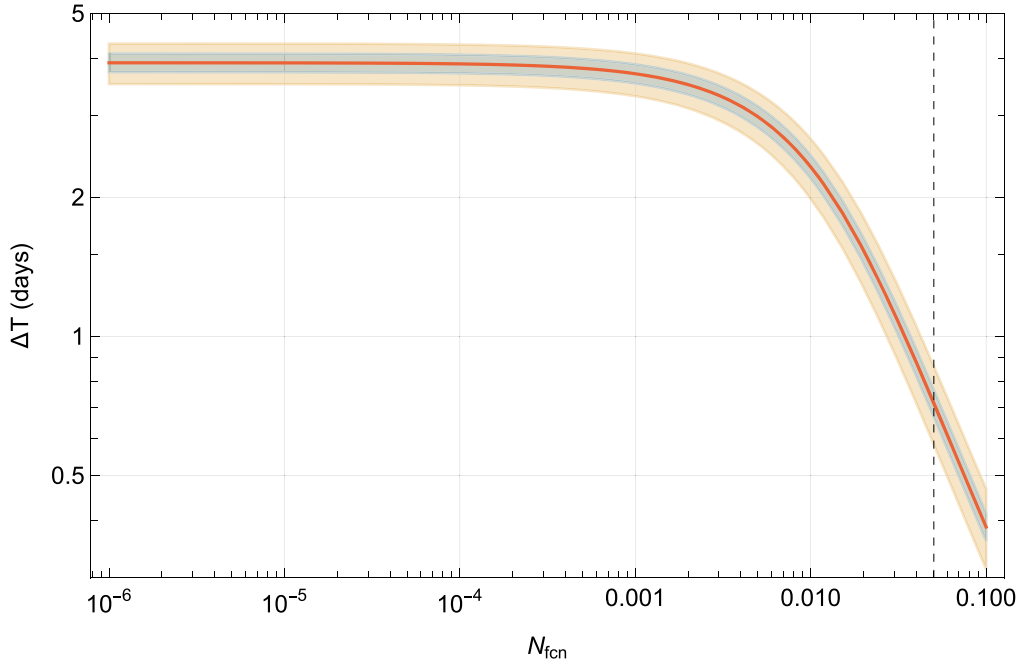

Figure 6. Period offset in the inertial frame, ΔT, as given by Equation (81) as a function of $N_{\rm fcn}$ (other parameters are from Table 1). The inner shaded area (in blue) corresponds to the interval of ± 10 days about $T_{\rm fcn}$, and the outer one (in yellow) to the interval of $\pm 10\%$ about $\mathrm{Im}(K_{\rm cmb})$. The vertical dashed line corresponds to Earth's value.

p. 131). This effect can be clearly observed from the comparison between the green and the yellow curves in Figure 5. The fact that $N_{\rm fcn} \to 0$ when $\delta \to 0$ follows immediately from Equation (74), but it is not so obvious from the approximate expression given by Equation (76). It becomes clearer when one realizes that this limit corresponds to having $A_{\rm f} \ll A_{\rm m}$ in Equation (77).

Using the above, the transfer function derived in Section 3.4 can be approximated by

$$T(\omega) \approx \frac{A}{A_{\rm m}} \frac{(e-\epsilon)}{e} \frac{(\omega - \bar{\omega}^{\epsilon}_{\rm som})}{(\omega - \bar{\omega}_{\rm fcn})} \tag{79}$$

$$\approx 1 + \frac{N_{\rm fcn}(1+\omega)}{(\omega - \bar{\omega}_{\rm fcn})}, \tag{80}$$

which is valid in the near-diurnal band where $\omega \approx -1$. Incidentally, note that Equation (80) satisfies the gyrostatic rigidity constraint exactly and that we could have arrived at it directly from Equation (72).

From Equation (68), we can compute the *period offset*, ΔT, in the inertial frame given by the formula

$$\Delta T \equiv T_{\rm max} - T_{\rm fcn} = \frac{\mathrm{Re}(\bar{\omega}_{\rm fcn}) - \omega_{\rm max}}{(1 + \mathrm{Re}(\bar{\omega}_{\rm fcn}))(1 + \omega_{\rm max})}. \tag{81}$$

The result is shown in red in Figure 6 as a function of $N_{\rm fcn}$, for the parameters of Table 1. We see that ΔT gets larger for decreasing values of $N_{\rm fcn}$ before reaching a plateau corresponding to the limit of Equation (70). From Equation (81), we see that the level of this plateau depends on the values of both $T_{\rm fcn}$ and $\mathrm{Im}(K_{\rm cmb})$ through $\mathrm{Re}(\bar{\omega}_{\rm fcn})$ and $\mathrm{Im}(\bar{\omega}_{\rm fcn})$, respectively. The inner shaded area of the figure (in blue) corresponds to the interval of ± 10 days about the value of $T_{\rm fcn}$ derived from Table 1. Similarly, the outer shaded area (in yellow) corresponds to the interval of $\pm 10\%$ about $\mathrm{Im}(K_{\rm cmb})$. Those deviations are far bigger than current uncertainties in measurements and are here provided as an indication of the weak dependence of ΔT on these quantities. The vertical dashed line corresponds to the best-fit value of $N_{\rm fcn}$ for Earth.

4.3. Implications for Mars and the Moon

Closer values of $\bar{\omega}_{\rm fcn}$ and $\bar{\omega}^{\epsilon}_{\rm som}$ lead to a larger offset, ΔT, between the resonance period, $T_{\rm max}$, and $T_{\rm fcn}$. From Equation (78), we therefore expect this offset to be larger in situations where $N_{\rm fcn} \ll 1$ and $T_{\rm fcn} \to \infty$. From Equation (76), we see that this first condition corresponds to $A_{\rm f}/A_{\rm m} \ll 1$. For Mars, this ratio is expected to be roughly of the same order of magnitude as in Earth, and $T^{\delta}_{\rm fcn} \approx -240$ days (Folkner et al. 1997; Van Hoolst et al. 2000). Furthermore, since Mars has no intrinsic global magnetic field, the dissipation at the CMB is mainly viscous and so probably much smaller than in Earth. Therefore, we expect ΔT to be negligible for this planet, to the effect that the observed resonance period can be safely equated to $T_{\rm fcn}$ and used as such to constrain the basic rotation parameters.

The situation is different for the Moon, where lunar laser ranging (LLR) measurements give $A_{\rm f}/A \approx 7 \times 10^{-4}$, $e_{\rm f} \approx 2.2 \times 10^{-4}$, and $\mathrm{Im}(K_{\rm cmb}) \approx -2.34 \times 10^{-5}$ (Williams et al. 2014), the latter value being computed from the formula given by Organowski & Dumberry (2020). Note that the flow at the Moon's CMB is likely turbulent (Williams et al. 2001), so that the latter parameter is proportional to $|m_{\rm f}|$ (Yoder 1981; Cébron et al. 2019). Since the Moon's spin rate is much slower than Earth's, it is more useful to give the ratio $\Delta T/T_{\rm fcn}$, which in the limit of $N_{\rm fcn}$ and $\mathrm{Im}(K_{\rm cmb})$ small approximates to

$$\frac{\Delta T}{T_{\rm fcn}} \to -\frac{|\mathrm{Im}(K_{\rm cmb})|}{e_{\rm f}}, \tag{82}$$

which is about −10% for the Moon. Equation (82) could, in principle, be used as an independent means to measure $\mathrm{Im}(K_{\mathrm{cmb}})$. This is something that might, however, prove difficult, as the FCN period is both very long and poorly constrained at the moment: $T^{\mathbb{C}}_{\mathrm{fcn}} \approx -374 \pm 93$ yr (Viswanathan et al. 2019). In addition, as we have already noted, having $N_{\mathrm{fcn}} \ll 1$ considerably reduces the amplitude of the resonance. Indirect observation of the FCN based on its resonance with weaker modes of physical libration has been proposed (Barkin et al. 2014; Petrova et al. 2018). Our results show that such measurements would not give $T^{\mathbb{C}}_{\mathrm{fcn}}$ directly, but rather a value 10% smaller. A possible way to obtain this mode's frequency directly would be to combine measurements of ω_{max} and ω_{min} with Equations (70) and (71).

4.4. Implications for Earth's Secular Evolution

Throughout this work, we have treated the parameters of Table 1 as constants. While this is certainly true on the timescales relevant for geodetic observation, these parameters might have changed significantly throughout Earth's evolution. Greff-Lefftz & Legros (1999a, 1999b) examined modulations in the FCN frequency caused by changes in the ratio of moments of inertia and in the CMB flattening over geological timescales, as well as the secular deceleration of the axial spin rate, Ω_0, caused by the lunar tidal torque. They identified the latter as the dominant source of FCN modulation, which could have caused episodes of increased dissipation at the CMB by "tuning" the FCN into resonance with the lunisolar tidal waves. They argued that such an episode might be correlated to major geological events. They also estimate that secular variations of K_{cmb} could not have significantly influenced this tuning mechanism, given the weak dependence of $\mathrm{Re}(\omega_{\mathrm{fcn}})$ on this parameter. It might be worthwhile to revisit that argument in light of the present study, especially given the strong dependence of the frequency offset on the value of $\mathrm{Im}(\mathrm{K}_{\mathrm{cmb}})$.

4.5. Conclusion

In the present work, we have looked in detail at the differences between the SOM and the FCN. We elaborated on the fact that, despite their similarity, those two motions are not the same thing and that they are free modes of two different systems, namely, that of a fluid core inside a steadily rotating mantle and that of the whole planet when the mantle can wobble freely. Focusing on that later system subjected to an external tidal forcing, we have shown that the frequency of the SOM retains some significance in the nondissipative freely rotating model and corresponds to that where the external torque on the mantle is exactly balanced by that produced by the core at the CMB, thereby leaving the free mantle in a state of steady rotation. When dissipation is reintroduced, we have shown that the peak of the resonance of the forced nutations with the FCN is slightly offset by a value of ≈ -1 day for Earth. We explained how this can be interpreted mathematically as the result of the presence of a complex zero of the transfer function at the frequency of the SOM close to the pole at the FCN frequency. We demonstrated how the offset is larger when these two frequencies are very close to each other. Based on that, we showed that this offset is likely to be negligible for Mars but could be more important for the Moon ($\approx -10\%$ of the FCN frequency). We also briefly discussed how this result might have been different in other periods during Earth's evolution.

In future work, it might be interesting to reconsider the above formalism based on the transfer function and how it may relate to the work of Triana et al. (2019), who showed that the FCN may interact in a complex way with other inertial modes present in the viscous core of Earth when their frequencies are close. This is something that may help cast light on some of the remaining elusive properties of inertial modes coupled to planetary rotation.

The author would like to thank Prof. V. Dehant, Prof. T. Van Hoolst, and Dr. S. A. Triana for the very useful discussions throughout the writing of this work. He is also thankful to the two reviewers, Profs. B. Buffett and M. Dumberry, whose comments and careful reviews helped to significantly improve the manuscript. J.R. acknowledges funding by the European Research Council under the European Unions Horizon 2020 research and innovation program (GRACEFUL, Synergy Grant agreement No. 855677).

Appendix A
Transformation between Inertial and Rotating Frames

We can parameterize the *passive* transformation relating the components of a vector, $\boldsymbol{v}$, in the inertial frame coordinates, $\{V^x, V^y, V^z\}$, to the components of the same vectors in the body frame coordinates, $\{v^x, v^y, v^z\}$, as

$$\begin{pmatrix} v^x \\ v^y \\ v^z \end{pmatrix} = \underbrace{R_3(-\gamma)\cdot R_2(-\beta)\cdot R_1(-\alpha)\cdot R_3(-\Omega_0 t)}_{T} \begin{pmatrix} V^x \\ V^y \\ V^z \end{pmatrix}, \quad \text{(A1)}$$

where $\{R_i(\theta)\}$ is the set of the usual three-dimensional matrix representation of rotation by an angle θ,

$$\begin{aligned} R_1(\theta) &= \begin{pmatrix} 1 & 0 & 0 \\ 0 & \cos\theta & -\sin\theta \\ 0 & \sin\theta & \cos\theta \end{pmatrix}, \\ R_2(\theta) &= \begin{pmatrix} \cos\theta & 0 & -\sin\theta \\ 0 & 1 & 0 \\ \sin\theta & 0 & \cos\theta \end{pmatrix}, \\ R_3(\theta) &= \begin{pmatrix} \cos\theta & -\sin\theta & 0 \\ \sin\theta & \cos\theta & 0 \\ 0 & 0 & 1 \end{pmatrix}. \end{aligned} \quad \text{(A2)}$$

The three Euler angles, α, β, and γ, relate the coordinates in the body frame to those in the frame rotating steadily at the diurnal frequency (SRF; see above). They are related to the components of the angular velocity, $\boldsymbol{\Omega}$, via dynamical relations and must therefore be treated as first-order quantities in agreement with the limit $|\boldsymbol{m}| \ll 1$. Based on Equation (A1), we can immediately compute the components of the vector $\hat{\boldsymbol{Z}}$ used in Equation (9) of Section 2.1 in the body frame to be $(-\beta, \alpha, 1)^{\top}$. From the time-dependent transformation matrix, T, in Equation (A1), we can define the rotation tensor:

$$\underline{\boldsymbol{R}} \equiv \frac{dT}{dt}\cdot T^{\top}. \quad \text{(A3)}$$

This tensor is antisymmetric. Its dual vector defines the angular velocity of the transformation T, which must be equal to $\boldsymbol{\Omega}$, by definition (see, e.g., Arnol'd 1989, for details). Solving for α,

β, and γ gives (in Fourier space)

$$\alpha = -\frac{(i\omega m^x + \Omega_0 m^y)\Omega_0}{\omega^2 - \Omega_0^2}, \quad \beta = \frac{(-i\omega m^y + \Omega_0 m^x)\Omega_0}{\omega^2 - \Omega_0^2}, \quad \gamma = 0. \tag{A4}$$

Upon reintroducing into Equation (A1), we find

$$\tilde{v} = \tilde{V} e^{-i\Omega_0 t}, \tag{A5}$$

where we have defined $\tilde{v} = (v^x + iv^y)$ and $\tilde{V} = (V^x + iV^y)$ as usual. From Equation (A5), we see that there is a diurnal phase difference between the components of any vector, $\boldsymbol{v}$, measured in the rotating frame and the same components measured in the inertial frame. Note that this result is consistent with the first component of Equation (23), the latter representing an *active* rotation of a vector in a fixed system of coordinates.

The nutation vector has Cartesian components in the inertial frame given by $(X, Y, 0)^\top$, where X and Y denote the equatorial coordinates of Earth's North Pole with respect to the Celestial Reference Frame of J2000 (see Dehant & Mathews 2015b). By definition, the rate of change of this vector must be equal to $\boldsymbol{\Omega} \times \boldsymbol{r}$. Using Equation (A5), we therefore arrive at

$$\Omega_0 \tilde{m} = i\frac{d\tilde{\eta}}{dt} e^{-i\Omega_0 t}, \tag{A6}$$

where we have defined $\tilde{\eta} = X + iY$. One must exert caution when computing the time derivative, $d\tilde{\eta}/dt$. In Fourier space we have

$$\Omega_0 \tilde{m}(\omega) e^{i\omega t} = i\frac{d}{dt}(\tilde{\eta}(\omega) e^{i\omega t}) e^{-i\Omega_0 t} \tag{A7}$$

$$= -\omega \tilde{\eta}(\omega) e^{i(\omega - \Omega_0)t}, \tag{A8}$$

from which we see that the individual Fourier component of frequency ω in the wobble, $\tilde{m}(\omega)$, is proportional to the individual Fourier component of frequency $(\omega + \Omega_0)$ in the nutation, $\tilde{\eta}(\omega + \Omega_0)$. *In extenso*,

$$\tilde{\eta}(\omega + \Omega_0) = -\frac{\tilde{m}(\omega)}{\omega + \Omega_0}\Omega_0. \tag{A9}$$

This expression becomes infinite for $\omega = -\Omega_0$, corresponding to the resonance with the TOM (see Section 2.4).

Appendix B
Spin-over Solution from the Momentum Equation of Fluid Dynamics

The momentum equation of a fluid in the frame rotating at angular velocity, $\boldsymbol{\Omega}$, given by Equation (8) is written as, to first order in the velocity and in the Fourier space,

$$i\omega(\boldsymbol{v} + \boldsymbol{m} \times \boldsymbol{r}) + 2\boldsymbol{\Omega} \times \boldsymbol{v} = -\boldsymbol{\nabla} p, \tag{B1}$$

where p and $\boldsymbol{v}$ denote the (reduced) pressure and the velocity of the fluid, respectively. The latter can be written using the ansatz given by Equation (10). The scalar function, ψ, is then chosen to accommodate the "no-penetration" boundary condition at the CMB:

$$\boldsymbol{v} \cdot \hat{\boldsymbol{n}}|_{\partial\mathcal{V}} = 0 \tag{B2}$$

$$\leftrightarrow \hat{\boldsymbol{n}} \cdot \boldsymbol{\nabla}\psi|_{\partial\mathcal{V}} = -\hat{\boldsymbol{n}} \cdot (\boldsymbol{\omega} \times \boldsymbol{r})|_{\partial\mathcal{V}}, \tag{B3}$$

where $\partial\mathcal{V}$ is the surface boundary of the fluid volume, $\mathcal{V}$, with normal vector $\hat{\boldsymbol{n}}$. The incompressibility condition, $\boldsymbol{\nabla} \cdot \boldsymbol{v} = 0$, imposes that ψ must be a harmonic function of the coordinates, i.e., $\nabla^2\psi = 0$. Poincaré (1910) computed this function for the fluid ellipsoid with dimensions (a, b, c). In the special case where $b = a$, using Equation (11), it is written as

$$\psi = \Omega_0 \frac{a^2 - c^2}{a^2 + c^2}(m_f^y x - m_f^x y)z \tag{B4}$$

$$= \Omega_0 e_f (m_f^y x - m_f^x y)z, \tag{B5}$$

where we have used the definition $e_f = (C_f - A_f)/A_f$, where A_f, and C_f are the equatorial and polar moments of inertia of the axisymmetric fluid ellipsoid,

$$A_f = M_f \frac{(a^2 + c^2)}{5}, \quad C_f = 2M_f \frac{a^2}{5}, \tag{B6}$$

where $M_f = (4\pi/3)\rho_f a^2 c$ is the ellipsoid's mass and ρ_f is its density.

Taking the curl of Equation (B1), we have, to first order in $\boldsymbol{m}$ and $\boldsymbol{m}_f$,

$$i\omega(\boldsymbol{m} + \boldsymbol{m}_f) = \hat{\boldsymbol{z}} \times \boldsymbol{m}_f + \Omega_0^{-1}(\hat{\boldsymbol{z}} \cdot \boldsymbol{\nabla})\boldsymbol{\nabla}\psi. \tag{B7}$$

Plugging in Equation (B5), the equatorial components of Equation (B7) can be combined into

$$\tilde{m}\omega = -\tilde{m}_f(\omega + (1 + e_f)\Omega_0), \tag{B8}$$

which, upon solving for $\tilde{m}_f$, gives us Equation (36). If we replace e_f by its expression in terms of the ellipsoid's dimensions, we recover the familiar expression for the SOM frequency of fluid dynamics (Greenspan 1968):

$$\omega_{som} = -\frac{2a^2}{a^2 + c^2}\Omega_0. \tag{B9}$$

In this form, we see that the SOM frequency is proportional to the ratio of the polar and equatorial moments of inertia.

ORCID iDs

Jérémy Rekier https://orcid.org/0000-0003-3151-6969

References

Arnol'd, V. 1989, Mathematical Methods of Classical Mechanics (Berlin: Springer)
Backus, G., & Rieutord, M. 2017, PhRvE, 95, 053116
Barkin, Y. V., Hanada, H., Matsumoto, K., Sasaki, S., & Barkin, M. Y. 2014, SoSyR, 48, 403
Buffett, B. A. 1992, JGR, 97, 19581
Buffett, B. A., Mathews, P. M., & Herring, T. A. 2002, JGRB, 107, 2070
Busse, F. H. 1968, JFM, 33, 1
Chao, B.F., & Hsieh, Y. 2015, E&PSL, 432, 483
Cébron, D., Laguerre, R., Noir, J., & Schaeffer, N. 2019, GeoJI, 219, S34
Cébron, D., Le Bars, M., & Meunier, P. 2010, PhFl, 22, 116601
Dehant, V., Laguerre, R., Rekier, J., et al. 2017, Geodesy and Geodynamics, 8, 389
Dehant, V., & Mathews, P. 2015a, Treatise on Geophysics (Amsterdam: Elsevier), 263
Dehant, V., & Mathews, P. M. 2015b, Precession, Nutation and Wobble of the Earth (Cambridge: Cambridge Univ. Press)
Deleplace, B., & Cardin, P. 2006, GeoJI, 167, 557
Dumberry, M., & Koot, L. 2012, GeoJI, 191, 530
Folkner, W. M., Yoder, C. F., Yuan, D. N., Standish, E. M., & Preston, R. A. 1997, Sci, 278, 1749
Franklin, G. F., Powell, J. D., & Emami-Naeini, A. 1994, Feedback Control of Dynamic Systems (Reading, MA: Addison-Wesley)
Greenspan, H. P. 1968, The Theory of Rotating Fluids, Cambridge Monographs on Mechanics and Applied Mathematics (London: Cambridge Univ. Press)
Greff-Lefftz, M., & Legros, H. 1999a, GeoJI, 139, 131

Greff-Lefftz, M., & Legros, H. 1999b, Sci, 286, 1707
Hough, S. 1895, RSPTA, 186, 469
Ivers, D. 2017, GApFD, 111, 333
Ivers, D. J., Jackson, A., & Winch, D. 2015, JFM, 766, 468
Koot, L., Dumberry, M., Rivoldini, A., De Viron, O., & Dehant, V. 2010, GeoJI, 182, 1279
Landau, L. D., & Lifshitz, E. M. 1969, Mechanics—Volume 1 of Course of Theoretical Physics (Oxford: Pergamon Press)
Le Bars, M., Cébron, D., & Le Gal, P. 2015, AnRFM, 47, 163
Mathews, P. M., Buffett, B. A., Herring, T. A., & Shapiro, I. I. 1991, JGR, 96, 8219
Mathews, P. M., & Guo, J. Y. 2005, JGRB, 110, B02402
Mathews, P. M., Herring, T. A., & Buffett, B. A. 2002, JGRB, 107, 2068
Munk, W. H., & MacDonald, G. J. 1960, The Rotation of the Earth: A Geophysical Discussion (Cambridge: Cambridge Univ. Press)
Nobili, C., Meunier, P., Favier, B., & Bars, M. L. 2021, JFM, 909, A17
Noir, J., Cardin, P., Jault, D., & Masson, J. P. 2003, GeoJI, 154, 407
Noir, J., & Cébron, D. 2014, JFM, 737, 412
Organowski, O., & Dumberry, M. 2020, JGRE, 125, e06386
Petrova, N. K., Nefedyev, Y. A., Zagidullin, A. A., & Andreev, A. O. 2018, ARep, 62, 1021
Poincaré, H. 1910, BuAsI, 27, 321
Rekier, Jérémy, Chao, Benjamin F., Chen, Jianli, et al. 2022, SGeo, 43, 149
Rekier, J., Triana, S. A., Trinh, A., & Dehant, V. 2020, PSJ, 1, 20
Rogister, Y. 2001, GeoJI, 144, 459
Sasao, T., Okubo, S., & Saito, M. 1980, in IAU Symp. 78, Nutation and the Earth's Rotation (Dordrecht: Reidel), 165
Smith, M. L. 1977, GeoJ, 50, 103
Smith, M. L., & Dahlen, F. A. 1981, GeoJI, 64, 223
Toomre, A. 1974, GeoJ, 38, 335
Triana, S. A., Rekier, J., Trinh, A., & Dehant, V. 2019, GeoJI, 218, 1071
Van Hoolst, T., Dehant, V., & Defraigne, P. 2000, P&SS, 48, 1145
Viswanathan, V., Rambaux, N., Fienga, A., Laskar, J., & Gastineau, M. 2019, GeoRL, 46, 7295
Wahr, J. M. 1981, GeoJ, 64, 705
Wahr, J. M. 1984, JGR, 89, 7621
Williams, J. G., Boggs, D. H., Yoder, C. F., Ratcliff, J. T., & Dickey, J. O. 2001, JGR, 106, 27933
Williams, J. G., Konopliv, A. S., Boggs, D. H., et al. 2014, JGRE, 119, 1546
Yoder, C. F. 1981, RSPTA, 303, 327
Zhu, P., Rivoldini, A., Koot, L., & Dehant, V. 2017, Geodesy and Geodynamics, 8, 427